Pramana – J. Phys. (2022) 96:190
https://doi.org/10.1007/s12043-022-02430-y

A study of topological characterisation and symmetries for a quantum-simulated Kitaev chain

Y R KARTIK[1,2], RANJITH R KUMAR[1,2], S RAHUL[1,2] and SUJIT SARKAR[1,*]

[1]Theoretical Sciences Division, Poornaprajna Institute of Scientific Research, Bidalur, Bengaluru 562 164, India
[2]Graduate Studies, Manipal Academy of Higher Education, Madhava Nagar, Manipal 576 104, India
*Corresponding author. E-mail: sujit.tifr@gmail.com

MS received 23 September 2021; revised 8 March 2022; accepted 5 May 2022

Abstract. An attempt is made to quantum simulate the topological characterisations, such as winding number, geometric phase and symmetry properties for a quantum-simulated Kitaev chain. We find that α (ratio between the spin–orbit coupling and magnetic field) and the range of momentum space of consideration, play crucial roles in topological classification. We show explicitly that, for this quantum-simulated Kitaev chain, the topological quantum phase transition occurs for finite range of momentum. We observe that the quasiparticle mass of the fermion plays a significant role in topological quantum phase transition. We also show that the symmetry properties of the simulated Kitaev chain is the same as that of the original Kitaev chain. The exact solution of the simulated Kitaev chain is given. This work provides a new perspective on new emerging quantum simulator and also for the topological state of matter.

Keywords. Kitaev chain; symmetry; topological state of matter.

PACS Nos 03.65.Vf; 61.50.Ah

1. Introduction

Quantum simulation process is a very prominent field of research now and in the foreseeable future. One aim of quantum simulation is to simulate a quantum system using a controllable laboratory system which underlines the same analytical models. Therefore, it is possible to simulate a quantum system that can be neither efficiently simulated on a classical computer nor can be easily accessed experimentally [1–13]. New, emerging quantum simulators will support creative, cutting-edge research in science to uncover different physical phenomena. The physics of Hamiltonian engineering is a major part of the quantum simulation process to study the behaviour of the system. It should be possible to engineer a set of interactions with external field or between different particles with tunable strength [12,13].

Intrinsic topological superconductors are quite rare in nature. However, one can engineer topological superconductivity by inducing effective p-wave pairing in materials which can be grown in the laboratory. One possibility is to induce proximity effect in topological insulators [14]; another is to use hybrid structures of superconductors and semiconductors [15–17].

If the researchers develop a hybrid system in a quantum nanowire which belongs to the same symmetry class as p-wave superconductor, then the hybrid system shows the same topological properties. This is the main theme/idea that motivated the scientists to propose many platforms which fulfill the requirements for simulating this physics and also the experimentalists to propose it.

In condensed matter physics, the Majorana fermion is an emergent quasiparticle zero-energy state [18,19]. The fundamental aspects of Majoranas and their non-Abelian braiding properties [20] offer possible applications in quantum computation [21–24]. Experimental realisation of Majorana fermions is a crucial step towards practical application of the quantum computing. Very recently, there have been many evidences of experimental signature [25–27] of Majorana fermions.

There are efforts in exploring the interplay of topology and symmetry in the tight band structures [28–39]. Arpit Raj *et al* [40] explored the rigidity of the topological invariant with the spontaneous breakdown of

Published online: 27 September 2022

protecting symmetries. Based on the properties of the ten-fold symmetry classification, each discrete symmetry involves some aspects of topological protection. In ref. [40], the researchers studied the evolution of topological invariant once such protecting symmetry breaks. There are some other works which mention about the emergence of some new symmetry classes (under interaction) [38], topological behaviour under external interaction [39] and geometric-curvature properties [41]. However, in this paper, we consider a very particular example of the simulated Kitaev chain to understand its momentum space characterisation as well as to make a comparison with the standard Kitaev chain results. Lutchyn *et al* [15] and Oreg *et al* [16] outlined the necessary ingredients for engineering a nanowire device that should contain a pairs of Majorana modes. The main aims of this letter are the topological characterisation in momentum space, symmetries and the exact solutions of the quantum-simulated Kitaev chain. The experimentalists will be motivated by the results of this quantum-simulated Kitaev chain. This work provides a new perspective on the new emerging quantum simulator and the topological state of matter.

2. Engineering the simulated Hamiltonian

Here, we consider a one-dimensional quantum wire with Rashba spin–orbit coupling (u), applied magnetic field (B) and couple to an s-wave superconductor with proximity-induced pairing (Δ).

$$H_1 = \left(\frac{k^2}{2m} + uk\sigma_x - \mu\right)\tau_z - B\sigma_z + \Delta\tau_x. \tag{1}$$

Spin–orbit coupling is along the x-direction which is perpendicular to the applied magnetic field (z-direction). We present the τ and σ operators in particle–hole space and spin space, and the analytical expressions for the τ and σ operators are explained in Appendix A. The first term is the kinetic energy term, which leads to the topological superconducting phase that makes the difference with the topological insulator Hamiltonian.

At first, we neglect the spin–orbit coupling ($B \gg u$). Then the dispersion relation becomes

$$\epsilon_k = \frac{k^2}{2m} \pm B,$$

i.e., we get the vertically shifted parabola for the up and down spin with an energy separation $\sim 2B$ (see figure 1a).

In figure 1b, two shifted parabola in the presence of Rashba spin–orbit interaction are shown. This corresponds to the topological insulator limit without Zeeman field. In this limit, the dispersion is

$$\epsilon_k = \frac{k^2}{2m} \pm uk.$$

Figure 1c shows the dispersion curves in the presence of both Zeeman field and spin–orbit interaction ($u > B$). This is the topological insulator limit in the presence of magnetic field. It produce a gap at the crossing point of two parabola of size $2B$. In this limit, the dispersion is [16]

$$\epsilon_k = \frac{k^2}{2m} \pm \sqrt{u^2k^2 + B^2}.$$

It is clear from the above equations that the spin–orbit coupling shifts the direction of the spin polarisation of the energy spectrum parabola from the Zeeman field direction. The tilting angle due to the presence of spin–orbit coupling is proportional to k. Therefore, the tilting angle is different (opposite) for the positive and negative momenta.

When we consider the chemical potential inside the gap, we observe that there is only one single left moving and single right moving electron and this limit is called the helical spin configuration which finally leads to the spinless p-wave superconductors [28–30]. We will see that the Zeeman field is not sufficient to quantum simulate the Kitaev chain but the spin–orbit interaction is also necessary to get the finite value of proximity-induced superconductivity. For finite Δ, the spectrum for constant μ, u, Δ and B is as follows:

$$E_\pm = \pm\sqrt{B^2 + \Delta^2 + {\epsilon_k}^2 + uk^2 \pm 2P}, \tag{2}$$

where

$$P = \sqrt{B^2\Delta^2 + B^2{\xi_k}^2 + u^2k^2{\xi_k}^2}, \quad \xi_k = \frac{k^2}{2m} - \mu.$$

Near $k \sim 0$

$$E_\pm(k \sim 0) = \pm\sqrt{B^2 + \Delta^2 + \mu^2 \pm 2B\sqrt{\Delta^2 + \mu^2}}.$$

It is very clear from the above expression that the gap closes at $k \sim 0$ at $B = \pm\sqrt{\Delta^2 + \mu^2}$ and the topological quantum phase transition occurs [15–17]. But we will prove explicitly that this relation does not hold for the Kitaev limit of the hybrid quantum nanowire and at the same time the transition does not occur at $k \sim 0$ but occurs for the consideration of finite range of momentum space during the topological phase transition process.

In figures 1d and 1e, we present the dispersion for the simulated Kitaev chain (eq. (4)) for two different values of u. Each figure consists of four curves, two of them are presented in red colour and the other two are presented in blue colour. The upper and lower red curves respectively represent the dispersion for the plus and minus sign in front of the square root of eq. (2). The upper and lower

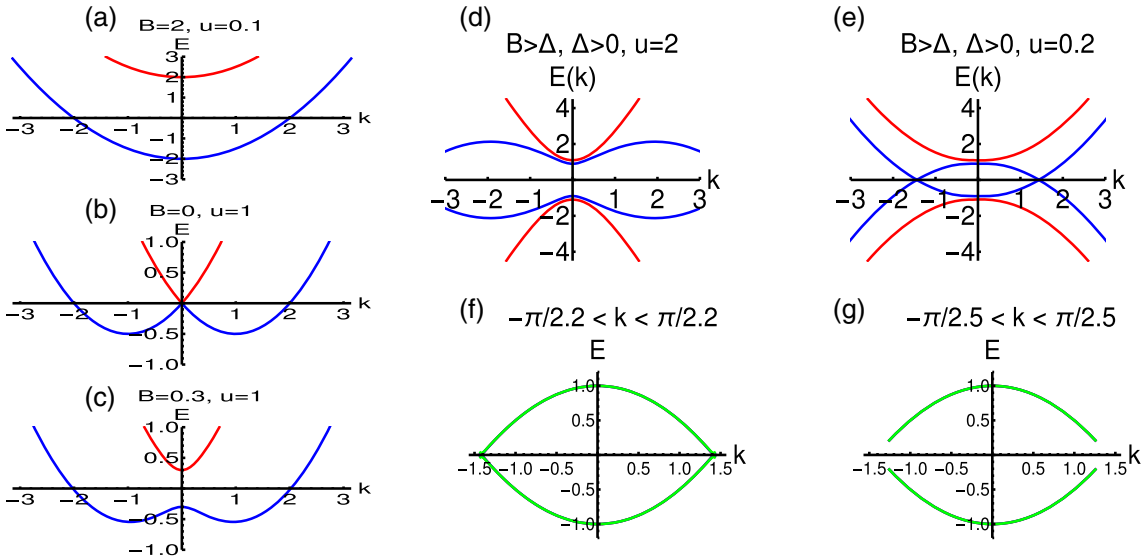

Figure 1. (**a**)–(**c**) The normal state ($\Delta = 0$) energy dispersion of the quantum nanowire (eq. (3)) for different limits of B and u depicting the Kitaev limit ($B \gg u$), topological insulator limit without and with magnetic field respectively. (**d**)–(**e**) The dispersion for different limit of eq. (2), for $\alpha = \{2, 0.2\}$ with $B = 1$ and $\Delta = 0.1$ respectively. (**f**)–(**g**) The dispersion of quantum-simulated Kitaev chain (eq. (4)) for different regimes of momentum with $\Delta = 0.1$ and $\alpha = \{0.02, 0.05, 0.2\}$ corresponding to red, blue and green colours respectively (here all the three lines overlap each other).

blue curves represent respectively the dispersion for the plus and minus sign within the square root of eq. (2).

These figures reveal that for higher values of u, there is always a gap in the dispersion spectrum but for lower values of $u = 0.2$, the lower and upper bands touch at $\pm k = \pi/2.2$. We will use this finding in the coming section to physically explain a few things.

The derivation of quantum-simulated Kitaev chain is a three-step process. At first, we consider the presence of magnetic field and the modification of kinetic energy (figure 1a). The second step is to find the effect of superconductivity on this dispersion. We show explicitly in Appendix A that the presence of spin–orbit interaction gives finite contribution p-wave superconductivity.

In this presentation, Δ is always finite and less than B and u. Here we derive the model Hamiltonian of the quantum nanowire in the Kitaev limit, i.e., the condition with the applied magnetic field (B) is much larger than the strength of spin–orbit coupling (u). Finally, we get the quantum-simulated Hamiltonian in the following form (please see Appendix A for the a detailed derivation).

$$H = \left(\frac{k^2}{2m} - \mu\right)\tau_z - \frac{uk}{2B}\Delta\tau_x. \tag{3}$$

The energy dispersion for this model Hamiltonian system is

$$E_k = \sqrt{\left(\frac{k^2}{2m} - \mu\right)^2 + \left(\frac{uk\Delta}{2B}\right)^2} = \sqrt{\left(\frac{k^2}{2m} - \mu\right)^2 + \frac{\alpha^2 k^2 \Delta^2}{4}}. \tag{4}$$

Thus, it is very clear that the effect of spin–orbit coupling has the effect to generate the p-wave pairing. The most important contribution of quantum wire with high magnetic field is the emergence of the topological superconducting phase. In the present study, we define a parameter $\alpha = u/B$, i.e, the ratio between the strength of the spin–orbit coupling and the applied magnetic field and the other parameter is the consideration of momentum space region, which is less than the full Brillouin zone. We will see that these two parameters play the role for the topological quantisation for the quantum-simulated Kitaev chain.

We present the dispersion of quantum-simulated Kitaev chain in figures 1f and 1g (eqs (3) and (4)) for two different ranges of momentum space. This figure shows that for this $\frac{-\pi}{2.2} < k < \frac{\pi}{2.2}$ momentum space consideration, the dispersion is closed at the BZ boundary point and for the other dispersion, a gap closing occurs. We consider three different values of $\alpha(= 0.02, 0.05, 0.2)$ for each figure and the dispersion results merge.

3. Results of topological invariant number with physical explanations

At first, we present the results of Kitaev chain for bench marking the results of quantum-simulated Kitaev chain (eq. (1)).

$$H_1 = -t\sum_{i=1}^{N-1}({c_i}^{\dagger}c_i + \text{h.c.}) + \sum_{i=1}^{N-1}(|\Delta|c_i c_{i+1} + \text{h.c.}) - \mu\sum_{i=1}^{N}{c_i}^{\dagger}c_i.$$

One can also write the Hamiltonian as

$$h(k) = \boldsymbol{\chi}(k)\cdot\boldsymbol{\tau},$$

where $\boldsymbol{\tau}$ are the Pauli matrices which act in the particle–hole basis, and $\chi_x(k) = 0$, $\chi_y(k) = 2\Delta\sin k$ and $\chi_z(k) = -2t\cos k - \mu$. Winding number is only an integer number and, therefore, cannot vary with smooth deformation of the Hamiltonian as long as the quasiparticle gap remains finite. At the point of topological phase transition, the winding number changes discontinuously. The analytical expression for winding number (W) for the Kitaev chain is

$$W = \left(\frac{1}{2\pi}\right)\int_{-\pi}^{\pi}\frac{2\Delta(2t+\mu\cos k)}{(\mu+2t\cos k)^2 + 4\Delta^2\sin^2 k}\mathrm{d}k$$

(detailed derivation is given in Appendix A).

In figure 2, we present the results for the winding number and also the energy dispersion for different ranges of momentum space consideration of the original Kitaev chain. This figure has two panels, and the upper and the lower panels respectively present the results for the first BZ ($-\pi < k < \pi$) and $\frac{-\pi}{2.2} < k < \frac{\pi}{2.2}$ momentum space consideration. The left and right figures for each panel are respectively for the winding number and energy dispersion for the corresponding momentum. We observe that the topological quantum phase transition occurs at $\mu = 2t$ in the upper panel but there is no such topological quantum phase transition for the lower panel. We observe that in figure 2c, energy gap disappears for topological quantum phase transition but there is no such transition for figure 2d. Thus, it is clear that the topological characterisation for the original Kitaev chain is related to the first BZ. One can also write the quantum-simulated Hamiltonian in the following form:

$$H_s = \begin{pmatrix}\chi_{sz}(k) & i\chi_{sy}(k)\\ -i\chi_{sy}(k) & -\chi_{sz}(k)\end{pmatrix},$$

where

$$\chi_{sz}(k) = \frac{k^2}{2m} - \mu, \quad \chi_{sy}(k) = \frac{uk\Delta}{2B},$$

$$\chi_{sz}(k) = \chi_z(-k), \quad \chi_{sy}(k) = -\chi_{sy}(-k),$$

$$\theta_{sk} = \tan^{-1}(\chi_{sz}(k)/\chi_{sy}(k)).$$

The analytical expression of the winding number for the simulated Kitaev chain is (we use the first expression of eq. (C1) to derive the winding number, please refer Appendix C for detailed information)

$$W_s = \frac{1}{2\pi}\int_{-\pi/a}^{\pi/a}\frac{m\alpha\Delta(k^2+2m\mu)\mathrm{d}k}{k^2m^2\alpha^2\Delta^2 + (k^2-2m\mu)^2},$$

where $\alpha = u/B$ and a is the number associated with the limit of different regions of momentum space consideration. a is 1 for the original Kitaev chain and takes different values for quantum-simulated Kitaev chain. We will see that this different limits of momentum space consideration leads to different topological quantum phase transition conditions.

In figure 3, We find that the topological quantum phase transition occurs at $\mu = 1/m$. It can be explained as follows: For small momentum, one can expand the cosine term as $1 - k^2/2$. Therefore, one can write the hopping integral as $t = 1/2m$ by using the dispersion relation. The parametric relation for topological quantum transition is $\mu = 2t = 1/m$. This figure reveals that the topological quantisation has started to work for the momentum space region $-\frac{\pi}{2} < k < \frac{\pi}{2}$. We observe that the topological quantisation occurs at $\mu = 1/m$. For the consideration of momentum space, $-\frac{\pi}{2.2} < k < \frac{\pi}{2.2}$, we term this region of momentum space as an effective Brillouin zone to quantum simulate the topological state of matter. Here we consider $\Delta = 0.1$. We justify this value of Δ in the description of exact solution (eq. (5)). Each figure consists of three curves for different values of α. We observe that as the value of α increases, i.e., the strength of the spin–orbit interaction increases, the quantisation condition for the topological quantum phase transition disappears. Thus, one can get the topological quantisation for the simulated Kitaev chain when the magnetic field is much higher than the spin–orbit coupling. This prediction is consistent with our consideration for smaller values of α during the quantum state engineering of simulated Kitaev chain.

Figure 4 shows the variation of winding number (W) with the quasiparticle mass. We find the same parametric relation for the topological quantum phase transition. We also observe that this transition occurs at $\mu = 1/m$ and as we approach smaller range of momentum space consideration, winding number drops sharply and touches the base line, i.e., in the limit $k = 0$, there is no topological quantum phase transition. To answer this, we should take a look at the topological phase transitions of quantum-simulated Kitaev chain at $k = 0$.

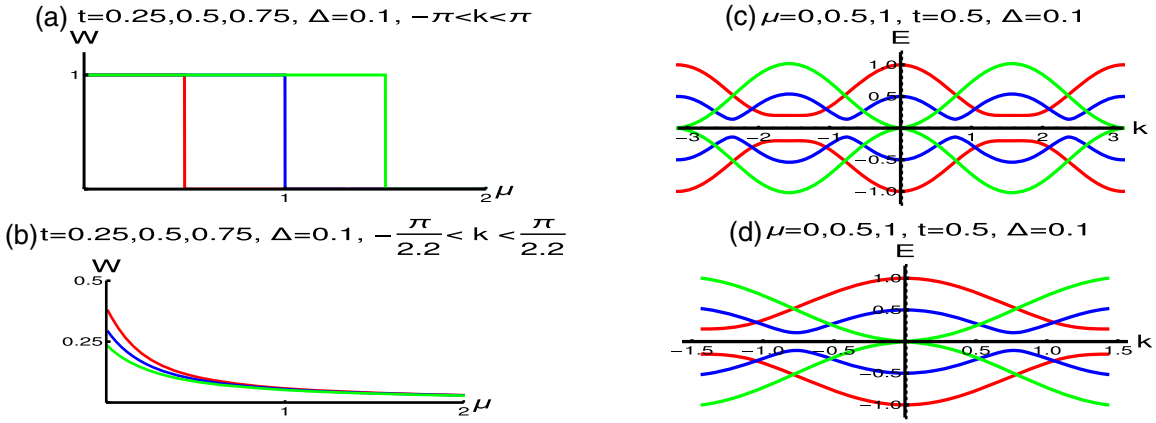

Figure 2. These figures present the winding number (left figure for each panel) and the energy dispersion (right figure for each panel) study of the original Kitaev chain. Each figure has three curves for different values of t as depicted in the figures. Here we consider $\Delta = 0.1$ and $m = 1$.

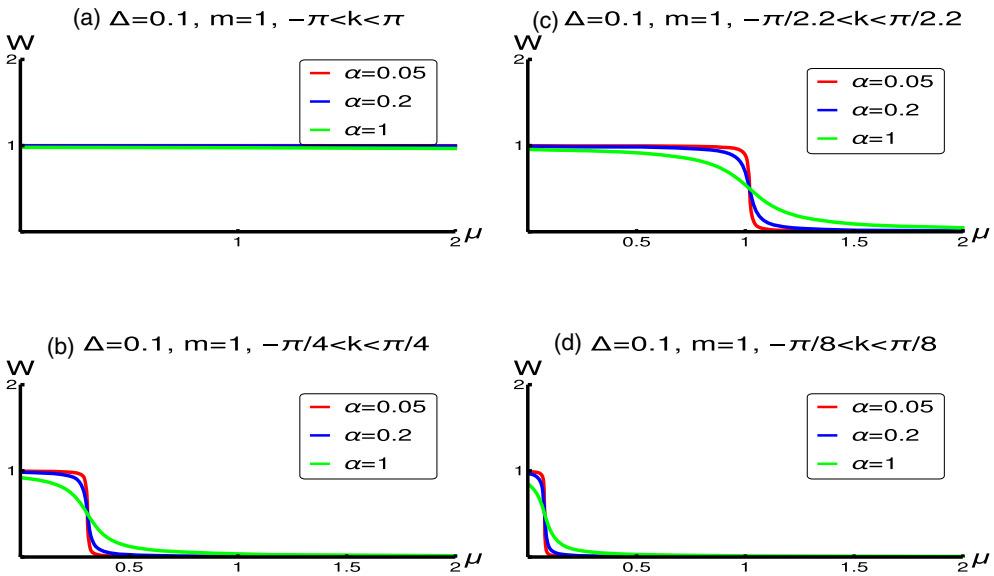

Figure 3. The variation of winding number with chemical potential for different regions of momentum space under consideration. Each figure consists of three curves for different values of α with $\Delta = 0.1$ and $m = 1$ as depicted in the figures.

$$\tilde{H} = \begin{pmatrix} -\mu & i\dfrac{uk\Delta}{2B} \\ -i\dfrac{uk\Delta}{2B} & \mu \end{pmatrix}.$$

$$W_s = \left(\frac{1}{2\pi}\right)\frac{u\Delta(2B-\mu)}{u^2\Delta^2}\arctan(k/\beta),$$

where

$$\beta = \frac{4B^2\mu^2}{u^2\Delta^2}.$$

Thus, it is clear from the above expression of simulated winding number that it goes to zero as the momentum goes to zero (detailed derivation is given in Appendix A).

4. Order of the phase transition

Topological transitions are the second-order (continuous) quantum phase transitions when they occur between two gapped phases. i.e., the second-order derivative of the ground-state energy shows a discontinuity in the parameter space.

$$E''(\mu) = \left(-\frac{1}{2\pi}\right)\int_{-\frac{\pi}{a}}^{\frac{\pi}{a}} \frac{\partial^2 E}{\partial \mu^2}\mathrm{d}k$$

with E being the ground-state energy, is a function of parameter μ. In a many-body system, $E = -\sum_k E_k$

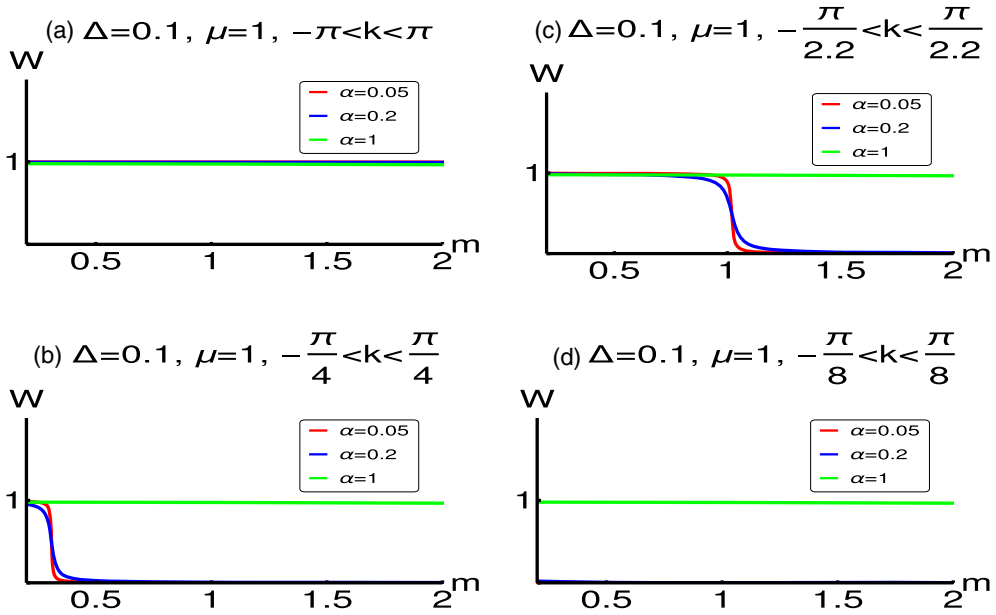

Figure 4. The variation of winding number with m for different regions of momentum space under consideration. Each figure consists of three curves for different values of α as depicted in the figures. Here we consider $\Delta = 0.1$ and $\mu = 1$. But all the curves coincide and finally green colour appears.

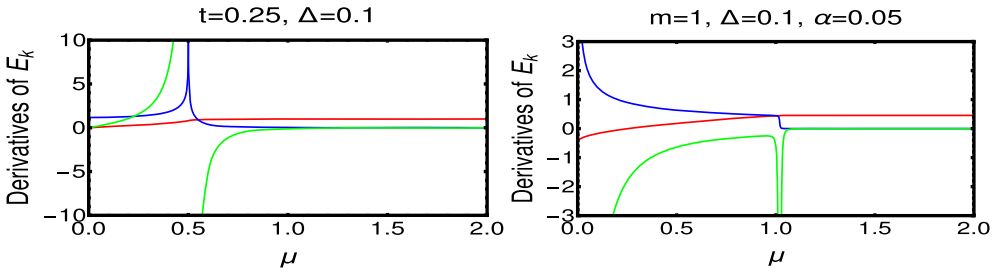

Figure 5. The order of phase transition in the original Kitaev (left) and simulated Kitaev (right) Hamiltonians. The red, blue and green curves respectively represent first-, second- and third-order derivatives with respect to μ.

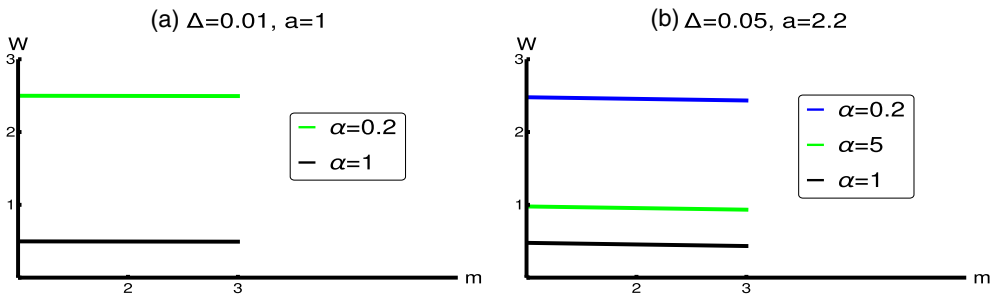

Figure 6. The results of exact solution for eq. (5). This figure consists of two panels for different regions of momentum space of consideration. The left and right panels are for the momentum space region $-\pi < k < \pi$ and $-\pi/2.2 < k < \pi/2.2$ respectively. Each figure has three different curves for different values of α as depicted in the figures.

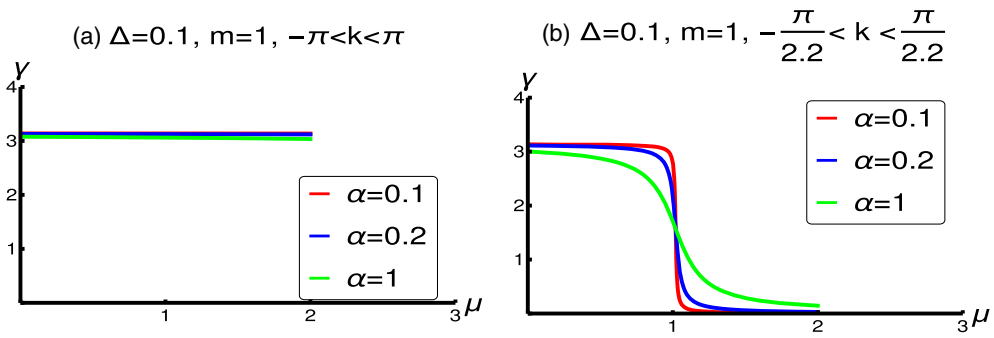

Figure 7. The variation of γ with μ for different regimes of momentum space for the simulated Kitaev chain. The other parameter space of these figures are also depicted in the figures.

Table 1. Different symmetry operations of the simulated Kitaev chain.

Symmetry	Operation	Result
$(\hat{\Theta})$	$\hat{\Theta}^{\dagger}\hat{H_{BdG}}(k)\hat{\Theta} = H(k)$	P
$(\hat{\Xi})$	$\hat{\Xi}^{\dagger}\hat{H}(k)\hat{\Xi} = (\sigma_x\hat{K})^{\dagger}\hat{H}(k)(\sigma_x\hat{K}) = \hat{K}^{\dagger}\sigma_x\hat{H}(k)\sigma_x\hat{K} = -\hat{H}(k)$	P
$(\hat{\Pi})$	$\hat{\Pi}^{\dagger}\hat{H_{BdG}}(k)\hat{\Pi} = \sigma_x\hat{H_{BdG}}(k)\sigma_x = -\hat{H}(k)$	P
$(\mathbb{P})$	$PH(k)P^{-1} = \sigma_z H(k)\sigma_z = H(-k)$	P
$(\mathbb{PT})$	$PTH(k)(PT)^{-1} \neq H(k)$	A
$(\mathbb{CP})$	$CPH(k)(CP)^{-1} = \sigma_x K\sigma_z H(k)\sigma_z K^{-1}\sigma_x = -H(-k)$	P
$(\mathbb{CT})$	$CTH(k)(CT)^{-1} = \sigma_x H(k)\sigma_x = -H(k)$	P
$(\mathbb{CPT})$	$\alpha H(k)\alpha^{-1} = \sigma_x\sigma_z K H(k) K^{-1}\sigma_z\sigma_x \neq -H(k)$	A

The symbols represent the corresponding mentioned symmetries. Time reversal $(\hat{\Theta})$, charge-conjugation $(\hat{\Xi})$, chiral $(\hat{\Pi})$, parity $(\mathbb{P})$, parity–time $(\mathbb{PT})$, charge conjugation–parity $(\mathbb{CP})$, charge conjugation–time reversal $(\mathbb{CT})$, charge conjugation–parity–time reversal $(\mathbb{CPT})$. The letters P and A represent the results *Present* and *Absent* respectively

[42,43] and the summation can be replaced with an integration for the Brillouin zone limit. The order of the discontinuity shows the order of the phase transition as the discontinuity spike represents the non-analiticities in the ground-state energy [44–47]. In figure 5, the ground-state energy is given by eq. (5) and its derivatives are taken with respect to parameter μ. For the original Kitaev chain, the second-order derivative of the ground-state energy shows the discontinuity while for the simulated Kitaev chain it is the third order. This shows that the phase transition in simulated Kiteav chain is of third order and the points $-\frac{\pi}{2.2}, \frac{\pi}{2.2}$ are the points, where the third-order derivative of the ground-state energy shows the discontinuity. Thus, in the limit $-\frac{\pi}{2.2} < k < \frac{\pi}{2.2}$ the simulated Kitaev chain shows a third-order continuous phase transition while the discrete symmetry properties remain the same as that of the original Kitaev chain.

5. Exact solution of the simulated Kitaev chain

It is well known that the Kitaev chain has exact solution for $\mu = 0$, for $\Delta = t$. For this limit, the system is always in the topological state without any transition. One can understand this constant topological state without any transition for $\mu = 0$ from the parametric relation ($\mu = 2t$) also. Here, we present some exact solutions to quantum-simulated Kitaev chain (figure 6). Detailed analysis is given in Appendix B.

Therefore, it is also a challenge to check the existence of exact solution for the simulated Kitaev chain. The exact solution of the winding number is

$$W_{\text{exact}} = \frac{1}{\alpha\pi}\cot^{-1}\left(\frac{2m\alpha\Delta}{a\pi}\right). \tag{5}$$

6. Geometric phase

The analytical expression for the geometric phase for the simulated Kitaev chain is as follows (detailed derivation is given in Appendix C):

$$\gamma_s = \frac{1}{2}\int_{-\pi/a}^{\pi/a} \frac{m\alpha\Delta(k^2 + 2m\mu)\mathrm{d}k}{k^2m^2\alpha^2\Delta^2 + (k^2 - 2m\mu)^2}.$$

In figure 7, we present the results of the geometric phase. The left and right figures are respectively for the

different values of momentum space region under consideration as depicted in figures. Each figure in the left panel consists of three curves for different values of hopping integral (t), and they satisfy the quantisation from finite value $\gamma(=\pi)$ to zero, i.e, the system drives from the topological state of matter to the non-topological state. It is very clear from this sfigure that the quantisation condition of γ appears when we consider the full BZ of the momentum space [31–36].

7. Symmetry presentation of the simulated Kitaev chain

Here we present the final results of the symmetry operations for this quantum-simulated model Hamiltonian. The detailed derivation is given in Appendix D. It is clear from table 1 that the symmetry properties of the simulated Kitaev chain and the original Kitaev chain are the same [37–40].

8. Conclusions

We have studied quantum-simulated Kitaev chain for a quantum nanowire with hybrid structure. We have presented results for topological quantisation and geometric phase of this simulated Kitaev chain. We have shown explicitly that topological characterisation in momentum space depends on two factors: the relative strength between the spin–orbit interaction and magnetic field and the consideration of momentum space region. We have shown that the symmetry of the quantum-simulated Kitaev chain is the same with the original Kitaev chain. We have observed a third-order quantum phase (continuous) transition in the simulated Kitaev chain, while the original Kitaev chain has showed second-order quantum phase transition. We have also presented the exact solution for the simulated Kitaev chain. This work provides a new perspective on new emerging quantum simulator and also the topological state of matter.

Acknowledgements

The author would like to acknowledge Prof. P K Mukherjee for reading the manuscript critically. The author also would like to acknowledge RRI library, DST for books and journals. YRK would like to thank Admar Mutt Education Foundation for the scholarship.

Appendix A. Derivation of Kitaev chain for a quantum nanowire

Kitaev limit can be achieved in the presence of strong magnetic field. Energy spectrum splits into two parabolic spectra for two different spin species, up and down and the chemical potential is inside the gap. The lower energy state is for the up-spin. The kinetic energy contribution is

$$H_{\text{kin}} = \left(\frac{k^2}{2m} - (B+\mu)\right)\tau_z. \tag{A.1}$$

At first we introduce six important operators.

$$\tau_x = \begin{pmatrix} 0 & 0 & 1 & 0 \\ 0 & 0 & 0 & 1 \\ 1 & 0 & 0 & 0 \\ 0 & 1 & 0 & 0 \end{pmatrix},$$

$$\tau_y = \begin{pmatrix} 0 & 0 & -i & 0 \\ 0 & 0 & 0 & -i \\ i & 0 & 0 & 0 \\ 0 & i & 0 & 0 \end{pmatrix},$$

$$\tau_z = \begin{pmatrix} 1 & 0 & 0 & 0 \\ 0 & 1 & 0 & 0 \\ 0 & 0 & -1 & 0 \\ 0 & 0 & 0 & -1 \end{pmatrix}.$$

Similarly, there are operators σ_x, σ_y and σ_z acting on the spin space.

$$\sigma_x = \begin{pmatrix} 0 & 1 & 0 & 0 \\ 1 & 0 & 0 & 0 \\ 0 & 0 & 0 & 1 \\ 0 & 0 & 1 & 0 \end{pmatrix},$$

$$\sigma_y = \begin{pmatrix} 0 & -i & 0 & 0 \\ i & 0 & 0 & 0 \\ 0 & 0 & 0 & -i \\ 0 & 0 & i & 0 \end{pmatrix},$$

$$\sigma_z = \begin{pmatrix} 1 & 0 & 0 & 0 \\ 0 & -1 & 0 & 0 \\ 0 & 0 & 1 & 0 \\ 0 & 0 & 0 & -1 \end{pmatrix}.$$

These operators τ_x, τ_y and τ_z are acting on the particle–hole space. Similarly, there are operators σ_x, σ_y and σ_z acting on the spin space. These six operators are mainly used for calculating the topological state of matter. Here we are simulating the Kitaev model for the spin-less fermion system. Therefore, we will use the operators τ's. In the next step, one can consider the pairing term. The low energy space of the BdG equation is spanned by the spin-up electron $|e\rangle = (1, 0, 0, 0)^T$ and the spin-up hole $|h\rangle = (0, 0, 0, 1)^T$. In this subspace of energy, there is no pairing term. The matrix elements, $\langle e|\Delta\tau_x|e\rangle =$

$$\langle h|\Delta\tau_x|e\rangle = \langle e|\Delta\tau_x|h\rangle = \langle h|\Delta\tau_x|h\rangle = 0.$$

$$\langle h|\Delta\tau_x|h\rangle = \Delta(0,0,0,1)\begin{pmatrix}0&0&1&0\\0&0&0&1\\1&0&0&0\\0&1&0&0\end{pmatrix}\begin{pmatrix}0\\0\\0\\1\end{pmatrix}$$

$$= \Delta(0,0,0,1)\begin{pmatrix}0\\1\\0\\0\end{pmatrix} = 0.$$

$$\langle e|\Delta\tau_x|e\rangle = \Delta(1,0,0,0)\begin{pmatrix}0&0&1&0\\0&0&0&1\\1&0&0&0\\0&1&0&0\end{pmatrix}\begin{pmatrix}1\\0\\0\\0\end{pmatrix}$$

$$= \Delta(1,0,0,0)\begin{pmatrix}0\\0\\1\\0\end{pmatrix} = 0.$$

$$\langle e|\Delta\tau_x|h\rangle = \Delta(1,0,0,0)\begin{pmatrix}0&0&1&0\\0&0&0&1\\1&0&0&0\\0&1&0&0\end{pmatrix}\begin{pmatrix}0\\0\\0\\1\end{pmatrix}$$

$$= 0 = \langle h|\Delta\tau_x|e\rangle.$$

Therefore, it is revealed from this study that the spin singlet pairing cannot induce proximity superconductivity in a perfectly spin-polarised system. This is also physically consistent because the spin singlet is possible only when the band is populated with up and down spin states.

Therefore, to get the finite contribution of superconductivity, we must have to consider the spin–orbit coupling, which modifies the energy spectrum and populates it with both up and down spins.

Now the spinors become

$$|e\rangle = \left(1, -\frac{uk}{2B}, 0, 0\right)^T$$

and

$$t|h\rangle = \left(0, 0, -\frac{uk}{2B}, 1\right)^T.$$

In this subspace, one can obtain

$$\langle h|\Delta\tau_x|e\rangle = \langle e|\Delta\tau_x|h\rangle = -\frac{uk}{2B}\Delta$$

and other matrix elements are zero.

$$\langle e|\Delta\tau_x|e\rangle$$

$$= \Delta\left(0, \frac{-uk}{2B}, 0, 0\right)\begin{pmatrix}0&0&1&0\\0&0&0&1\\1&0&0&0\\0&1&0&0\end{pmatrix}\begin{pmatrix}0\\\frac{-uk}{2B}\\0\\0\end{pmatrix}$$

$$= \Delta\left(0, \frac{-uk}{2B}, 0, 0\right)\begin{pmatrix}0\\0\\1\\-\frac{uk}{2B}\end{pmatrix} = 0 = \langle h|\Delta\tau_x|h\rangle.$$

$$\langle h|\Delta\tau_x|e\rangle$$

$$= \Delta\left(0, 0, \frac{-uk}{2B}, 0\right)\begin{pmatrix}0&0&1&0\\0&0&0&1\\1&0&0&0\\0&1&0&0\end{pmatrix}\begin{pmatrix}0\\\frac{-uk}{2B}\\0\\0\end{pmatrix}$$

$$= \Delta\left(0, 0, \frac{-uk}{2B}, 0\right)\begin{pmatrix}0\\0\\1\\-\frac{uk}{2B}\end{pmatrix}.$$

$$= -\Delta\frac{uk}{2B} = \langle e|\Delta\tau_x|h\rangle.$$

Therefore, the final form of the model Hamiltonian is

$$H \simeq \left(\frac{k^2}{2m} - \mu\right)\tau_z - \frac{uk}{2B}\Delta\tau_x.$$

This is the analogous form of the BdG Hamiltonian of a spin-less p-wave superconductor with the effective pairing $\Delta_{\text{eff}} = u\Delta/2B$. Therefore, we conclude that effective p-wave pairing is due to the presence of spin–orbit coupling and it becomes weak when Zeeman field is large [17].

Appendix B. Exact solution of the simulated Kitaev chain

It is well known that the Kitaev chain has exact solution for $\mu = 0$, for $\Delta = t$. For this limit, the system is always in the topological state without any transition. One can also understand this constant topological state without any transition for $\mu = 0$ from the parametric relation $\mu = 2t$.

Therefore, it is also a challenge to check the existence of exact solution for the simulated Kitaev chain. The exact solution of the winding number is

$$W_{\text{exact}} = \frac{1}{\alpha\pi}\cot^{-1}\left(\frac{2m\alpha\Delta}{a\pi}\right). \tag{B.1}$$

In figure 8, we present the exact result of W with the varying parameter m. Each panel consists of three figures for different values of Δ. The left panel has a BZ limit which runs from $-\pi$ to π. Here, we do not observe any topological state with integer winding number. In the right panel, we present exact solution with a reduced BZ limit from $-\pi/2.2$ to $\pi/2.2$. Here, we observe that

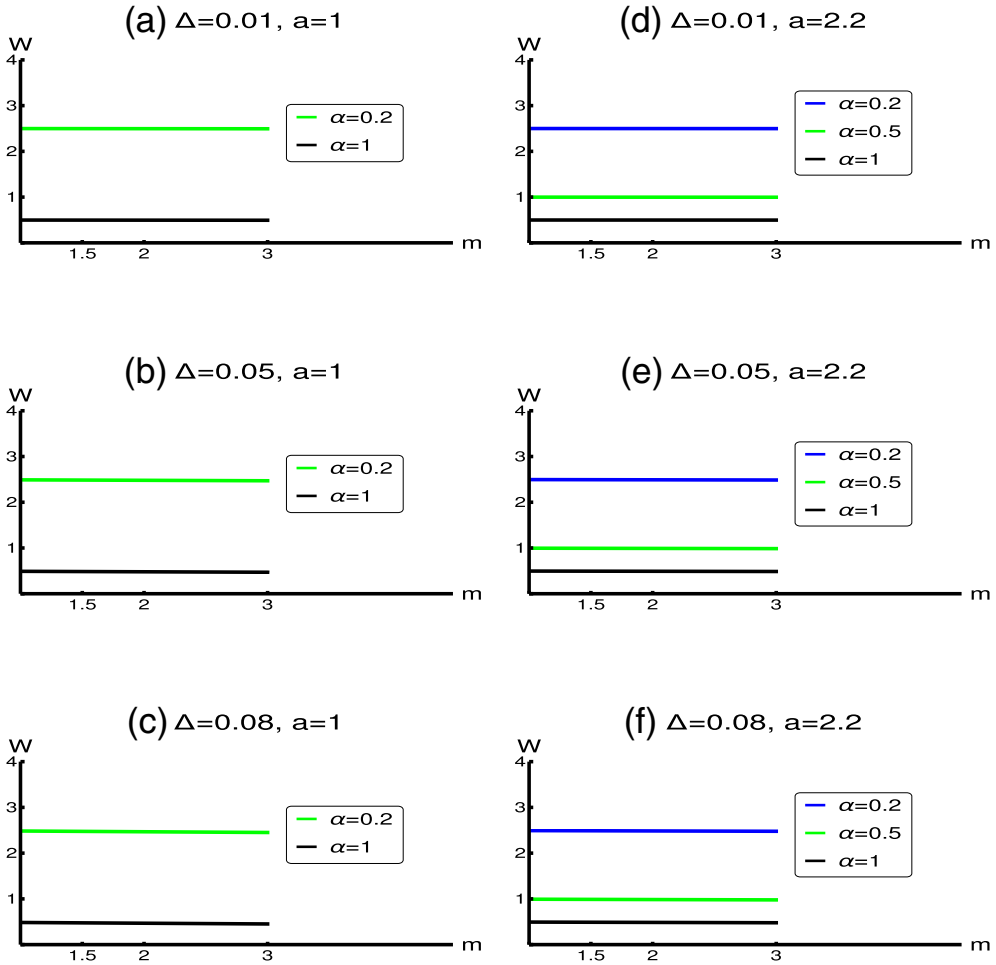

Figure 8. These figures present the exact solution for the quantum-simulated Kitaev chain with respect to m. The left panel represents the BZ with a boundary from $-\pi$ to π. The right panel represents the BZ with a boundary from $-\pi/2.2$ to $\pi/2.2$. Each figure consists of three curves for different values of Δ.

the system is in the topological state with winding number very close to $W_{\text{exact}} = 0.5$ for $\alpha = 1$. We observe that for higher values of Δ, the topological state do not remain constant with increasing values of m. It is clear from this study that one can also reproduce the exact solution of the Kitaev chain for smaller values of Δ by using the simulated Kitaev chain. This can be considered as an advantage with quantum-simulated Kitaev chain.

Appendix C. Results of geometric phase with physical explanation

At first, we describe very briefly the basic aspect of geometric phase. During the adiabatic time evolution of the system, the state vector acquires an extra phase over the dynamical phase, $|\psi(R(t))\rangle = \mathrm{e}^{\alpha_n}|\phi(R(t)\rangle$, where $\alpha_n = \theta_n + \gamma_n$. Here $\theta_n = \frac{-1}{\hbar}\int_0^t E_n(\tau)\mathrm{d}\tau$ and γ_n are the dynamical and geometric phases respectively. For a system, the geometric phase is given by the cyclic evolution of state vectors over a closed curve. It is evident from the analytical expression of Berry phase that it depends on the geometry of the parameter and loop (C) therein.

$$\gamma_n(C) = i\int_C \langle\phi(x)|\nabla|\phi(x)\rangle \mathrm{d}x.$$

The geometric (Zak) phase is an important concept for the topological characterisation of low-dimensional quantum many-body system [13,32,33]. Zak has considered the one-dimensional Brillouin zone and the cyclic parameter is the crystal momentum (k). The geometric phase in the momentum space is defined as

$$\gamma_n = \int_{-\pi}^{\pi} \mathrm{d}k\langle u_{n,k}|i\,\partial_k|u_{n,k}\rangle, \tag{C.1}$$

where $|u_{n,k}\rangle$ are the Bloch states which are the eigenstates of the nth band of the Hamiltonian. The simulated

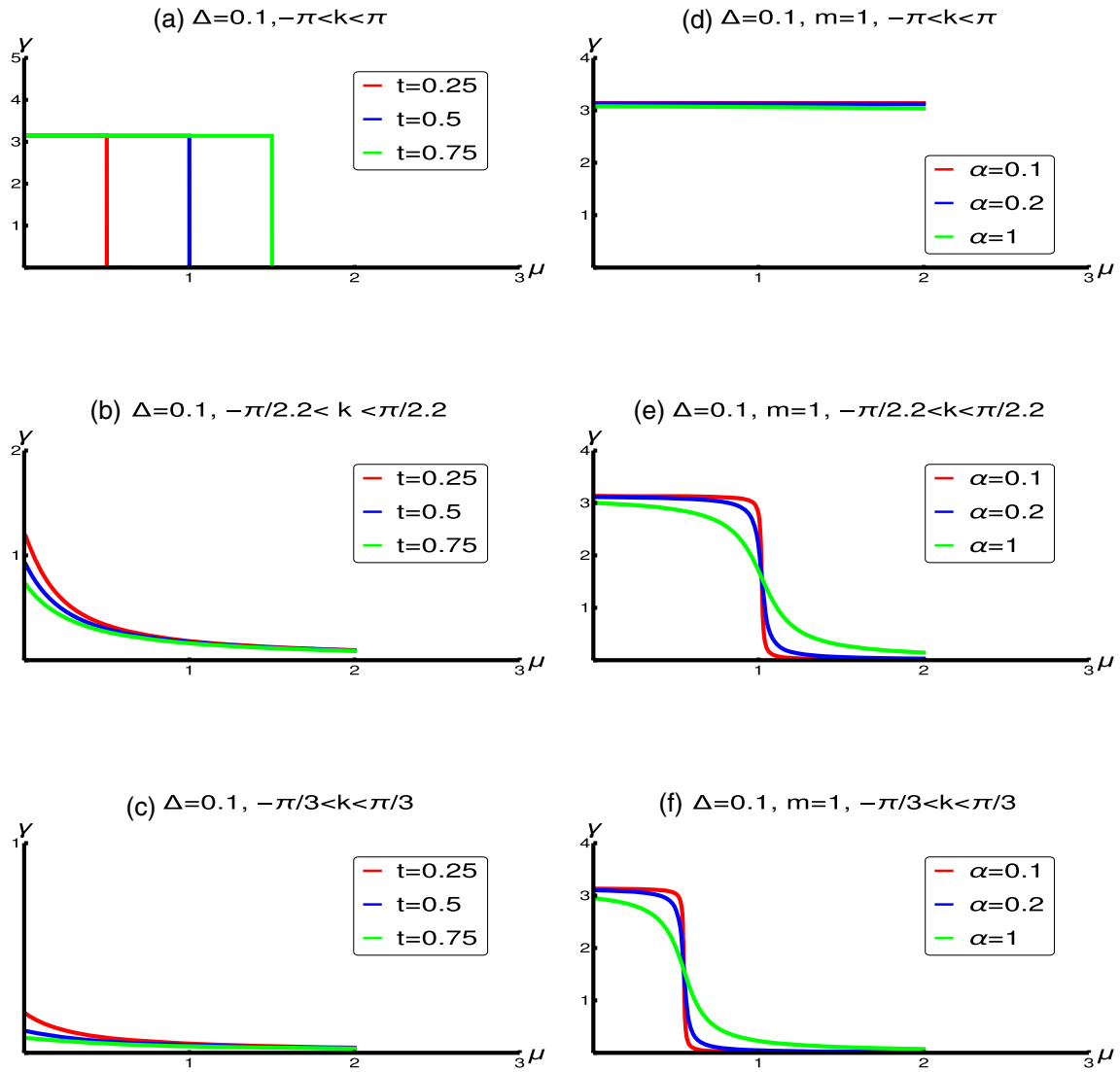

Figure 9. These figures present the behaviour of geometric phase with varying values of chemical potential. The left panel represents the original Kitaev chain and the right panel represents the simulated Kitaev chain. Each figure consists of three curves for different values of t as depicted in the figures. Here we consider $\Delta = 0.1$ and $m = 1$.

Kitaev chain possesses Z-type topological invariant and also the anti-unitary particle hole symmetry. For this system, the analytical expression of the Zak phase [13,32,33] is

$$\gamma = W\pi, \quad \text{mod } (2\pi). \tag{C.2}$$

In figure 9, we present the behaviour of γ with respect to μ. The left panel represents the variation of geometric phase for the original Kitaev chain with respect to the chemical potential where each curve represents different values of t. With increasing values of a, it is not possible to observe the topological phase transitions (Here a is the number associated with the limit of BZ. In general $a = 1$ for the original Kitaev chain and takes different values for simulated Kitaev chain). The right panel represents the variation of geometric phase for the simulated Kitaev chain with respect to the chemical potential. Here, each curve represents different values of α and it is also clear from this study that as we increase the value of α the quantisation condition for γ smeared out and there is no topological quantum phase transition for the simulated Kitaev chain.

It is revealed from the study of the right panel that γ shows the same behaviour of the original Kitaev chain when we consider the momentum space region $-\frac{\pi}{2.2} < k < \frac{\pi}{2.2}$. For the original Kitaev chain, the Bloch state traverse in the whole BZ whereas for the simulated Kitaev chain, the Bloch state traverses in the reduced momentum space as we see from the dispersion. For the consideration of momentum space region

$-\pi/2.2 < k < \pi/2.2$ for the simulated Kitaev chain, gives the same parametric relation of the original Kitaev chain for the topological phase transition.

Appendix D. An extensive derivation of symmetries for the simulated Kitaev chain

Among the vast variety of topological phases, one can identify an important class called symmetry-protected topological (SPT) phase, where two quantum states have distinct topological properties protected by certain symmetry. Under this symmetry constraint, one can define the topological equivalent and distinct classes. Hamiltonians which are invariant under the continuous deformation into one another preserving certain symmetries are the topological equivalent classes.

Different SPT states can be well understood with the local (gauge) non-spatial symmetries such as, time reversal (TR), particle–hole (PH) and chiral. In general, non-interacting Hamiltonians can be classified in terms of symmetries into ten different symmetry classes [34–37]. A particular symmetry class of a Hamiltonian is determined by its invariance under time-reversal, particle–hole and chiral symmetries. Apart from that, we also study the parity (P) symmetry, parity–time (PT) symmetry, charge conjugation–parity–time (CPT) symmetry, CP symmetry and CT symmetry. In this section, we present symmetry properties of the simulated Kitaev chain and also check how much it is equivalent with the original Kitaev chain. Here we present the final results of the symmetry operations for this quantum-simulated model Hamiltonian.

1: *Time-reversal symmetry*

Time-reversal symmetry operation is $\hat{\Theta}$. We use the properties of $\chi_z(k) = \chi_z(-k)$ and $\chi_y(k) = -\chi_y(-k)$.

$$\hat{\Theta}^\dagger \hat{H_{BdG}}(k)\hat{\Theta} = \hat{K}^\dagger \hat{H_{BdG}}(k)\hat{K} \cdot \hat{\Theta}^\dagger \hat{H_{BdG}}(k)\hat{\Theta}$$
$$= \hat{K}\begin{bmatrix} \chi_z(k) & i\chi_y(k) \\ -i\chi_y(k) & -\chi_z(k) \end{bmatrix}\hat{K} = H(k)$$
$$\chi_z(k) = \frac{k^2}{2m} - \mu, \quad \chi_y(k) = \alpha(= u/B)\Delta k.$$

Thus, the Hamiltonian obeys time-reversal symmetry.

2: *Charge-conjugation symmetry*

This symmetry operator is $\hat{\Xi}$.

$$\hat{\Xi}^\dagger \hat{H}(k)\hat{\Xi} = (\sigma_x \hat{K})^\dagger \hat{H}(k)(\sigma_x \hat{K}) = \hat{K}^\dagger \sigma_x \hat{H}(k)\sigma_x \hat{K},$$
$$\hat{\Xi}^\dagger \hat{H}(k)\hat{\Xi} = \hat{K}^\dagger \begin{pmatrix} 0 & 1 \\ 1 & 0 \end{pmatrix}\begin{pmatrix} \chi_z(k) & i\chi_y(k) \\ -i\chi_y(k) & -\chi_(k) \end{pmatrix}$$
$$\times \begin{pmatrix} 0 & 1 \\ 1 & 0 \end{pmatrix}\hat{K},$$
$$\hat{\Xi}^\dagger \hat{H}(k)\hat{\Xi} = \hat{K}\begin{pmatrix} -\chi_z(k) & -i\chi_y(k) \\ i\chi_y(k) & \chi_z(k) \end{pmatrix}\hat{K}$$
$$= \begin{pmatrix} -\chi_z(k) & -i\chi_y(k) \\ i\chi_y(k) & \chi_z(k) \end{pmatrix} = -\hat{H}(k).$$

Thus, the Hamiltonian obeys charge-conjugation symmetry.

3: *Chiral symmetry*

This symmetry operator is given by $\hat{\Pi}$.

$$\hat{\Pi}^\dagger \hat{H_{BdG}}(k)\hat{\Pi} = \sigma_x \hat{H}(k)\sigma_x$$
$$\hat{\Pi}^\dagger \hat{H}(k)\hat{\Pi} = \begin{pmatrix} 0 & 1 \\ 1 & 0 \end{pmatrix}\begin{pmatrix} \chi_z(k) & i\chi_y(k) \\ -i\chi_y(k) & -\chi_z(k) \end{pmatrix}\begin{pmatrix} 0 & 1 \\ 1 & 0 \end{pmatrix}$$
$$= -H(k).$$

Thus, the Hamiltonian also obeys chiral symmetry.

4: *Parity symmetry*

This symmetry operator is given by $\hat{P}$.

$$PH(k)P^{-1} = \sigma_z H(k)\sigma_z$$
$$= \begin{pmatrix} 1 & 0 \\ 0 & -1 \end{pmatrix}\begin{pmatrix} \chi_z(k) & i\chi_y(k) \\ -i\chi_y(k) & \chi_z(k) \end{pmatrix}\begin{pmatrix} 1 & 0 \\ 0 & -1 \end{pmatrix}$$
$$= H(-k).$$

Thus, the Hamiltonian obeys parity symmetry.

5: *PT symmetry*

This symmetry operator is given by $\hat{PT}$.

$$PTH(k)(PT)^{-1} = \sigma_z K H(k)K^{-1}\sigma_z = \sigma_z H(k)\sigma_z$$
$$= \begin{pmatrix} 1 & 0 \\ 0 & -1 \end{pmatrix}\begin{pmatrix} \chi_z(k) & i\chi_y(k) \\ -i\chi_y(k) & -\chi_z(k) \end{pmatrix}\begin{pmatrix} 1 & 0 \\ 0 & -1 \end{pmatrix}$$
$$= \begin{pmatrix} \chi_z(k) & -i\chi_y(k) \\ i\chi_y(k) & -\chi_z(k) \end{pmatrix} \neq H(k).$$

Thus, the Hamiltonian does not obey PT symmetry.

6: *CP symmetry*

This symmetry operator is given by $\hat{CP}$.

$$
\begin{aligned}
&CPH(k)(CP)^{-1} = \sigma_x K \sigma_z H(k) \sigma_z K^{-1} \sigma_x \\
&= \sigma_x K \begin{pmatrix} 1 & 0 \\ 0 & -1 \end{pmatrix} \begin{pmatrix} \chi_z(k) & i\chi_y(k) \\ -i\chi_y(k) & -\chi_z(k) \end{pmatrix} \\
&\quad \times \begin{pmatrix} 1 & 0 \\ 0 & -1 \end{pmatrix} K^{-1} \sigma_x \\
&= \sigma_x K \begin{pmatrix} \chi_z(k) & -i\chi_y(k) \\ i\chi_y(k) & -\chi_z(k) \end{pmatrix} K^{-1} \sigma_x \\
&= -H(-k).
\end{aligned}
$$

Thus, the Hamiltonian obeys CP symmetry.

7: *CT symmetry*

This symmetry operator is given by $\hat{CT}$.

$$CTH(k)(CT)^{-1} = \sigma_x H(k) \sigma_x = -H(k).$$

Thus, the Hamiltonian obeys the CT symmetry.

8: *CPT symmetry*

This symmetry operator is given by $\hat{\alpha}$.

$$
\begin{aligned}
&\alpha H(k) \alpha^{-1} = \sigma_x \sigma_z K H(k) K^{-1} \sigma_z \sigma_x \\
&= \begin{pmatrix} 0 & 1 \\ -1 & 0 \end{pmatrix} \neq -H(k).
\end{aligned}
$$

Thus, the Hamiltonian does not obey the CPT symmetry. Therefore, from this detailed derivation it is clear that the symmetry properties of the quantum-simulated Kitaev chain as well as original Kitaev chain are the same.

References

[1] R P Feynman, *Int. J. Theor. Phys.* **21**, 467 (1982)
[2] S Lloyd, *Science* **273**, 1073 (1996)
[3] I Buluta and F Nori, *Science* **326**, 108 (2009)
[4] I M Georgescu, S Ashhab and F Nori, *Rev. Mod. Phys.* **86**, 153 (2012)
[5] J I Cirac and P Zoller, *Nat. Phys*. **8**, 264 (2012)
[6] A Trabesinger, *Nat. Phys.* **8(4)**, 263 (2012)
[7] L Sanchez-Palencia, *C. R. Phys.* **19(6)**, 357 (2018)
[8] E Altman, K R Brown, G Carleo, L D Carr, E Demler, C Chin, B DeMarco, S E Economou, M A Eriksson, K-M C Fu, M Greiner, K R A Hazzard, R G Hulet, A J Kollár, B L Lev, M D Lukin, R Ma, X Mi, S Misra, C Monroe, K Murch, Z Nazario, K-K Ni, A C Potter, P Roushan, M Saffman, M Schleier-Smith, I Siddiqi, R Simmonds, M Singh, I B Spielman, K Temme, D S Weiss, J Vučković, V Vuletić, J Ye and M Zwierlein, *PRX Quantum* **2**, 017003 (2021)
[9] I Bloch, J Dalibard and S Nascimbene, *Nat. Phys.* **8**, 267 (2012)
[10] A Aspuru-Guzik and P Walther, *Nat. Phys.* **8**, 285 (2012)
[11] A A Houck, H E Türeci and J Koch, *Nat. Phys.* **8**, 292 (2012)
[12] S Sarkar, *EPL* **110**, 64003 (2015)
[13] S Sarkar, *Sci. Rep.* **7**, 1 (2017)
[14] L Fu and C L Kane, *Phys. Rev. Lett.* **100**, 096407 (2008)
[15] R M Lutchyn, J D Sau and S D Sarma, *Phys. Rev. Lett.* **105**, 77001 (2010)
[16] Y Oreg, G. Refael and F V Oppen, *Phys. Rev. Lett.* **105**, 177002 (2010)
[17] F von Oppen, Y Peng and F Pientka, *Lecture Notes of the Les Houches Summer School: Topological Aspects of Condensed Matter Physics* (Oxford Scholarship Online, 2017)
[18] A Y Kitaev, *PHYS-USP* **44**, 131 (2001)
[19] F Wilczek, *Nat. Phys.* **5**, 614 (2009)
[20] J Alicea, *Rep. Prog. Phys.* **75**, 076501 (2012)
[21] C W J Beenakker, *Annu. Rev. Condens. Matter Phys.* **4**, 113 (2012)
[22] A Y Kitaev, *Ann. Phys.* **303**, 2 (2003)
[23] B I Halperin, Y Oreg, A Stern, G Refael, J Alicea and F von Oppen, *Phys. Rev. B* **85**, 144501 (2012)
[24] J D Sau, D J Clarke and S Tewari, *Phys. Rev. B* **84**, 094505 (2011)
[25] V Mourik, K Zuo, S M Frolov, S R Plissard, E P A M Bakkers and L P Kouwenhoven, *Science* **336**, 1003 (2012)
[26] M T Deng, C L Yu, G Y Huang, M Larsson, P Caroff and H Q Xu, *Nano Lett.* **12**, 6414 (2012)
[27] A Das, Y Ronen, Y Most, Y Oreg, M Heiblum and H Shtrikman, *Nat. Phys.* **8**, 887 (2012)
[28] S Sarkar, *Sci. Rep.* **6**, 30569 (2016)
[29] R M Lutchyn and M P A Fisher, *Phys. Rev. B* **84**, 214528 (2011)
[30] A M Lobos, R M Lutchyn and S Sarma, *Phys. Rev. Lett.* **109**, 146403 (2012)
[31] P W Anderson, *Phys. Rev.* **110**, 827 (1958)
[32] J Zak, *Phys. Rev. Lett.* **62**, 2747 (1989)
[33] S Ryu and Y Hatsugai, *Phys. Rev. B* **73**, 245115 (2006)
[34] C-K Chiu, J C Y Teo, A P Schnyder and S Ryu, *Rev. Mod. Phys.* **88**, 035005 (2016)
[35] J Kruthoff, J de Boer, J van Wezel, C L Kane and R-J Slager, *Phys. Rev. X* **7**, 041069 (2017)
[36] L Fu, *Phys. Rev. Lett.* **106**, 106802 (2011)
[37] S Sarkar, *Sci. Rep.* **8**,1 (2018)
[38] R R Kumar and S Sarkar, *Ph. Transit.* **93**, 287 (2020)
[39] S Rahul, R R Kumar, Y R Kartik, A Banerjee and S Sarkar, *Phys. Scr.* **94**, 115803 (2019)
[40] A Raj, N Banerjee and T Das, *Phys. Rev. B* **103**, 075139 (2021)
[41] Y R Kartik, R R Kumar, S Rahul and S Sarkar, *Pramana – J. Phys.* **95**, 102 (2021)
[42] Y Niu, S B Chung, C-H Hsu, I Mandal, S Raghu and S Chakravarty, *Phys. Rev. B* **85**, 035110 (2012)
[43] M Malard, D Brandao, P E de Brito and H Johannesson, *Phys. Rev. Res.* **2**, 033246 (2020)

[44] P Cats, A Quelle, O Viyuela, M A Martin-Delgado and C M Smith, *Phys. Rev. B* **97**, 121106 (2018)
[45] S N Kempkes, A Quelle and C M Smith, *Sci. Rep.* **6**, 38530 (2016)
[46] SChen, L Wang, Y Hao and Y Wang, *Phys. Rev. A* **77**, 032111 (2008)
[47] Y R Kartik, R R Kumar, S Rahul, N Roy and S Sarkar, *Phys. Rev. B* **104**, 075113 (2021)